PSFC/JA-02-23

Resistive MHD Transport Model for an RFP Part II – Results

A. Bruno, J.P. Freidberg,* R.J. Hastie

October 2002

Plasma Science and Fusion Center
Massachusetts Institute of
Technology
Cambridge, MA 02139 USA

*Massachusetts Institute of
Technology
Department of Nuclear Engineering
Room 24-107
Cambridge, MA 02139

This work was supported by the U.S. Department of Energy, Grant No. DE-FG02-91ER-54109.

Submitted for publication to *Physics of Plasmas*

I Introduction

The second paper of the sequence presents a series of results obtained by numerically solving the resistive MHD marginal stability transport equations derived in Part I. Comparisons with experimental, theoretical, and computational studies are presented. Specifically, three different types of applications are considered.

First, direct comparisons of τ_E and β_p are made between the marginal stability model and RFP data obtained from the two existing main devices, MST and RFX. The agreement is reasonably good keeping in mind that the theoretical model has zero free parameters to adjust.

Second, scaling relations showing the dependence of τ_E and β_p on I, a, and n are presented. These are compared with other theories and computational models as well as experimental data, which is rather sparse at this point in time. The marginal stability model gives the most complete set of scaling relations to date. These relations predict the confinement behavior of any given device as parameters are varied and again agree reasonably well with the limited amount of data available. Future experiments are needed to further confirm or deny the accuracy of the model.

Third, the marginal stability model is used to interpret a widely used empirical curve obtained by Werley several years ago [1]. This curve predicts the maximum value of τ_E for any given device as a function of I, a, and n. At first glance the scaling dependence of Werley's empirical curve seems very different from the marginal stability scaling relations presented here. However, when a proper interpretation of "maximum τ_E" is invoked, there is again reasonable agreement.

Before proceeding with the results it is helpful to carefully define the two critical parameters τ_E and β_p used in the analysis. The definitions used are the standard ones. In particular, the formula for β_p is given by:

$$\beta_p \doteq \frac{4\mu_0}{a^2 B_{\theta a}^2} \int_0^a pr \; dr \tag{1}$$

where $B_{\theta a} = \mu_0 I / 2\pi a$, $p = nT$, and $T_e = T_i = T/2$. The steady state energy confinement time is defined in terms of the heat flux at the wall assuming that anomalous electron heat conduction is the primary loss mechanism

$$a\kappa_{\perp e} \left. \frac{\partial T}{\partial r} \right|_a \equiv -\frac{3}{\tau_E} \int_0^a pr \; dr \tag{2}$$

The steady state energy balance equation then gives

$$\tau_E \doteq \frac{3}{2} \frac{\int_0^a pr\ dr}{\int_0^a (\eta j^2 - p\nabla \cdot \mathbf{v})\, r\ dr} \tag{3}$$

The ohmic term can be expressed in terms of plasma equilibrium profiles (assuming for instance Spitzer's formula for plasma resistivity). However the evaluation of the dynamo term $p\nabla \cdot \mathbf{v}$ is quite complicated, requiring a knowledge of the nonlinear turbulent fluctuations. Note that under the assumption that these fluctuations are incompressible ($\nabla \cdot \mathbf{v} = \mathbf{0}$), the dynamo term exactly vanishes. It is easy to show that this term also vanishes if the adiabatic form of the energy equation is used. Neither of these conditions is valid for the present model.

Nevertheless, even without invoking incompressibility, or adiabaticity, there is some belief based on experimental data that the dynamo term might actually average out to zero when integrated over the plasma volume. That is, physically the dynamo transfers energy from one region of the plasma to another, but does not directly generate a large net energy loss. It is this belief coupled with complexity of explicitly dealing with the turbulent fluctuations that motivates the use of a simpler definition of energy confinement time, one in which the dynamo term is neglected

$$\tau_E \doteq \frac{3}{2} \frac{\int_0^a pr\ dr}{\int_0^a \eta j^2 r\ dr} \tag{4}$$

With these definitions, the resistive MHD marginal stability model has been solved for a wide number of cases. The results are discussed in the remainder of the text.

II Comparison with Standard RFP Experiments in MST and RFX

A comparison is made between the marginal stability model and standard RFP discharges for MST and RFX (whose characteristic parameters are listed in Table 1). A standard RFP discharge is defined as one in which there is no profile control, PPCD, or similar applied techniques aiming at improving the confinement. Note that the MST data are ensemble averages of similar discharges, combined to reconstruct the core temperature profile (see Ref. [2]),

while the RFX data corresponds more to the observed range of parameters in standard RFP operation.

The first step is to choose the plasma parameters in the model such that a fair comparison with the experiments can be made. Recall that the model has only three parameters that can be used to match experimental data: two of them correspond to the pair of plasma parameters that define Taylor's relaxed state, (i.e. μ and B_{z0}, or Φ_t and K_h, or Θ and I, and so on). The third parameter is the core plasma density (which is constant for $0 < r < r_2$). Each of these is a known physical quantity from the data. In practice the experimental values of toroidal flux, toroidal current and core density are used to determine B_{z0}, μ, and n_0. They are given in Table 2.

By numerically solving the model, one first finds the not unexpected general result that the poloidal number $m = 1$ is most stringent in terms of the marginal stability condition (see Fig. 1). This can be easily seen from the tearing-mode marginality condition (see Part I), which indicates that the pressure gradient is proportional to the square root of the poloidal number m. Fig. 1 also shows the curves for $\Delta'_{m=1}$ from Iteration I (zero pressure gradient) and Iteration II (containing the plasma pressure from Iteration I). Note that no significant changes occur by introducing the pressure, aside from a small difference around the axis. This region has a small impact on the pressure profile generated from Iteration I, since p' on axis is already very flat due to Suydam's marginality condition. Overall, the relative change in plasma pressure from Iteration I to Iteration II is less that 10%, so that Iteration II already shows good convergence.

In Figs. 2 and 3, the numerical temperature profiles for MST and RFX are shown, together with the radial locations of the various transition points in the model. In Figs. 4 and 5, the profiles for the self-consistent $\chi_\perp$ for MST and RFX are shown. Observe the area of low thermal transport around the reversal layer, corresponding to the best confinement region (steepest pressure gradient). Also the $\chi_\perp$ corresponding to resistive MHD marginal stability transport, as evaluated from the model, is typically about $20 - 60m^2/s$ throughout most of the plasma core. This is about two orders of magnitude larger than the classical value.

Finally, in Tables 3 and 4, the experimental confinement parameters given in Table 1 are compared with the results from the marginal stability model as well as other transport models. These comparisons show a reasonable agreement with the marginal stability model, in contrast to the predictions of the other transport models (i.e. classical perpendicular transport or transport

determined by Suydam's condition for marginal stability).

III Scaling Relations for τ_E and β_p

The second type of result obtained with the model is the extraction of scaling laws for τ_E and β_p. A large ($\sim$ 100) database of simulations has been constructed, by solving the resistive MHD marginal stability model. Each data point takes about two hours of computing time on a Sun Ultra5 workstation. Most of the time is spent calculating the detailed radial profile for Δ' on a fine grid ($\sim$ 500 grid points). For ease of comparison with experiments the quantities β_p and τ_E are expressed in terms of the following independent plasma parameters:

$$\begin{aligned} I &\doteq 2\pi \int_0^a j_z r \, dr = \frac{2\pi a}{\mu_0} B_{\theta a} \\ N &\doteq 2\pi \int_0^a n r \, dr \\ a &\rightarrow minor\ radius \\ \Theta &\doteq \frac{2\pi a B_{\theta a}}{\Phi_t} \end{aligned} \tag{5}$$

A multiple linear regression of the numerical data base leads to the following scaling relations:

$$\tau_E = I^{1.1} \cdot N^{-0.25} \cdot a^{1.6} \cdot G(\Theta) \tag{6}$$

$$\beta_p = I^{-0.75} \cdot N^{0.49} \cdot a^{-0.16} \cdot K(\Theta) \tag{7}$$

The model also explicitely determines the functions $G(\Theta)$ and $K(\Theta)$ as a function of Θ as shown in Figs. 6 and 7, respectively, for the parameters corresponding to the MST Standard Shot given in Table 2. Note that $G(\Theta)$ and $K(\Theta)$ are completely determined. There are no free parameters. Thus, the magnitude as well as the scaling is predicted for τ_E and β_p.

Note that varying Θ throughout its range, between Θ_{min} (given by the reversal condition) and Θ_{max} (given by the tearing-mode instability condition $\Delta'_0 > 0$ occurring somewhere in the plasma region at $\beta_p = 0$), leads to only a small change in β_p and τ_E. The scaling relations are only weakly dependent on Θ and show a broad peak around typical RFP operational values, implying

somewhat poorer confinement in the proximity of Θ_{min} and Θ_{max} . This is in reasonable agreement with experimental results (see Ref. [3]), where no strong effect of confinement performance versus Θ is observed.

IV Comparison with Other Transport Models

This section compares the results obtained from the resistive MHD marginal stability transport model, with the predictions and the scalings obtained from other transport models. Of particular interest are the quantitative differences in the predicted values of τ_E and β_p. Three different transport models are discussed. The first one assumes a plasma turbulence marginal stability model dominated by ideal interchange modes. This corresponds to replacing the tearing-mode marginal condition with its analogue for ideal interchange modes, the Suydam criterion. The second scenario assumes the transport to be purely classical, as described by Braginskii in Ref. [4]. The final type of transport is described by Bohm diffusion (see Ref. [5]). A brief physical description of each of these models is now presented.

A Ideal Interchange-Mode Dominated Transport

For this transport scenario, it is easy to show that the energy confinement time scales as follows

$$\tau_E = \frac{I^3 a^2}{N^{\frac{3}{2}}} \cdot G_S(\Theta) \ \ [sec] \tag{8}$$

while the beta poloidal scales as

$$\beta_p = K_S(\Theta). \tag{9}$$

Here the units are as usual $I[MA]$, $N[10^{20}m^{-1}]$, and $a[m]$. The coefficients G_S and K_S, given as functions of Θ, typically exceed the experimental values by a factor of about 4 for β_p and 40 for τ_E (see Tables 3 and 4 for specific comparisons). Note the strong scaling with I and N as compared to the resistive MHD model.

B Classical Transport

The classical model is obtained by assuming that the transport coefficients are given by Braginskii's expressions [4]. In this case, τ_E and β_p scale as follows

$$\begin{aligned} \tau_E &= \frac{I^3 \cdot a^2}{N^{\frac{3}{2}}} G_C(\Theta) \ \ [sec] \\ \beta_p &= K_C(\Theta) \end{aligned} \tag{10}$$

exactly coinciding with the scaling found for the ideal interchange-mode dominated transport model. Also the magnitudes, given by the coefficients G_C and K_C, are comparable (see Table 3 and 4). Thus, classical transport also significantly exceeds the experimental values.

C Transport described by Bohm Diffusion

An anomalous transport model was suggested by Bohm in 1949 (see Ref. [5]). He proposed the following scaling relation for the particle diffusion coefficient D

$$D = \frac{T}{16B}\,, \tag{11}$$

with T in $[eV]$ and B in [Tesla]. Even today, there is still no rigorous derivation of Eq. (11), in terms of a specific physical mechanism. Nevertheless, Bohm diffusion is frequently used as a test scaling relation for comparison with data in which the numerical coefficient is extracted by data fitting. For the present purpose of describing the Bohm-diffusion transport model, the same dependence given by Eq. (11) is assumed for the thermal diffusivity:

$$\chi_\perp = C\frac{T}{B}, \tag{12}$$

although no physical argument is available to justify the choice of a particular numerical coefficient C. Thus, only the scaling for τ_E and β_p is evaluated and compared with the other models. The scaling for confinement in the case of Bohm diffusion is

$$\tau_E \sim I^{\frac{1}{7}} N^{\frac{2}{7}} a^{\frac{9}{7}}\,, \qquad \beta_p \sim \frac{N^{\frac{5}{7}}}{I^{\frac{8}{7}} a^{\frac{2}{7}}} \tag{13}$$

The scaling law derived from Bohm diffusion essentially shows a very weak dependence of τ_E on I and N.

D Conclusions

The conclusions from this comparison are as follows. Both the marginally stable Suydam model and the classical Braginskii model yield the same scaling relation for τ_E and β_p. The confinement time $\tau_E \sim I^3$ indicates a strong favorable scaling with current, which seems incompatible with the observed behavior on any given experiment. Also, the magnitude of τ_E from each of these theories is very optimistic, exceeding the experimental values by more than an order of magnitude.

The Bohm scaling relation is very pessimistic in that τ_E is almost independent of current. Also, there is no way to theoretically determine the multiplicative constant in front of the scaling relation.

In summary, none of these theories accurately describes the experimental data.

V Comparison with Recent Experimental and Computational Work

Here, a comparison is made between two recent papers whose aim was to provide a transport scaling relation for an RFP.

A 3D Model by Scheffel and Schnack

The first study (see Ref. [6]) is a computational analysis carried out by Scheffel and Schnack in 2000. They have implemented a 3D, resistive MHD code, using classical transport coefficients (including thermal conduction and viscosity). No radiation losses, or resistive wall effects are taken into account. Even though classical values for $\chi_\perp$ and $\chi_{||}$ are used, an anomalous global transport ($\chi_\perp$) is generated by parallel transport due to field line stochasticity in the core region.

This code is certainly more comprehensive than the one developed in the present model, not only because of the geometry and the presence of the plasma viscosity, but because of its nonlinear treatment of resistive MHD instabilities. Even so, there are limitations in Scheffel and Schnack's study.

First, only the scaling dependence on I and N are extracted, and not a and Θ, due to the long computing time required for each simulation. Second, the actual regression was performed on I^2/N, rather than on I and N separately. The scaling law found by Scheffel and Schnack is given by

$$\tau_E \sim \left(\frac{I^2}{N}\right)^{0.34} \quad , \quad \beta_p \sim \left(\frac{N}{I^2}\right)^{0.40} \tag{14}$$

The ratio I^2/N originates from the fact that the parameters used in the linear regression were a form of local plasma beta and local Lunquist number (which is defined as the ratio of the resistive diffusion time to the Alfven transit time): β_0 and S_0 in their notation. It is easy to show that both of these parameters scale with I^2/N. Notice that the definition of τ_E in the 3D code by Scheffel and Schnack takes into account the dynamo term.

B MST Experimental Scaling

The second study (see Ref. [2]) is an experimental analysis of confinement discharges, carried out by the MST group in 1998. By using a large database of discharges, they have generated a direct fit of experimentally measured velocity and magnetic field fluctuations in the MST device. Here again, the fit was carried out using the Lunquist number S, for the purpose of comparing experiments with theoretical scaling predictions of fluctuations (see Refs. [7],[8]). The following dependence has been extracted from the data

$$B_{1r} \sim S^{-0.2} \tag{15}$$

In order to determine a scaling relation for τ_E and β_p from this experimental fit, a theoretical assumption of dominant stochastic magnetic field diffusivity is made. This implies the following relation between τ_E and β_p (see Ref. [2])

$$\tau_E \sim \beta_p^{0.1} \left(\frac{I^2}{N}\right)^{0.3} \tag{16}$$

corresponding to the specific power law scaling given by Eq. (15). Equation (16), together with the basic relation arising from the definitions of τ_E and β_p

$$\tau_E \sim \beta_p^{\frac{5}{2}} a^2 \left(\frac{I^2}{N}\right)^{3/2} \tag{17}$$

lead once again to a scaling with I^2/N. Specifically, the MST scaling relations resulting from this analysis are

$$\tau_E \sim \left(\frac{I^2}{N}\right)^{0.25} \quad , \quad \beta_p \sim \left(\frac{N}{I^2}\right)^{0.5} \tag{18}$$

C The Comparison

Next, a comparison is made of the different scalings just presented, with the resistive MHD marginal stability model. In Figs. 8 and 9 experimental confinement data from three MST standard discharges (see Ref. [9]) are plotted versus I^2/N along with the various scaling relations.

The data corresponding to the three discharges plotted in these figures are listed in Table 5. Discharge 1 is the MST standard discharge already used in this chapter for earlier comparisons. The other two discharges (discharge 2 and discharge 3) have been recently reported by the MST group in Ref. [9]: they essentially have the same plasma density, while they differ in the plasma current by a factor of two. All of these discharges have a value of Θ of about $1.7 - 1.8$. Moreover, all the parameters were measured between sawtooth crashes, which occur regularly throughout standard MST plasmas, and which temporarily degrade the confinement.

It is worth emphasizing that the scaling relations predicted by the resistive MHD marginal model determine not only the dependence of τ_E and β_p on I, N, and a, but also the magnitude, given as a function of Θ. In contrast, both the MST scaling relation and the 3D model only give a prescription for the dependence on I and N. Hence, in order to be plotted in Figs. 8 and 9 the magnitudes of the MST and 3D scaling relations have been chosen to match the first experimental value. The resistive MHD marginal stability scaling relation uses the self consistent magnitude factor predicted by the theory.

A comparison of these results shows that all three theoretical scalings exhibit a similar but weak scaling of τ_E and β_p with I^2/N. The experimentally measured values of β_p agree reasonably well with the theoretical scaling predictions. The experimental values of τ_E show a somewhat weaker dependence with I^2/N than the theoretical predictions. The present marginal stability model predicts the magnitude of τ_E and β_p to within a factor of 2, a large improvement over the previous theoretical predictions discussed in Sec. IV, which were optimistic by more than one order of magnitude.

VI Comparison with the "best performance" scaling relation

In this section a comparison is made between the present theory and the often quoted "best performance" scaling relation first observed by Werley [1]. At first glance the scaling relations between the two theories appear to be quite different with the present theory indicating a much weaker (and hence unfavorable) scaling with I. However, as shown below, when the definition of "best performance" is taken into account, both scaling relations become quite similar.

A The Connor-Taylor scaling relation

Since the best performance scaling relation is similar to the one derived by Connor and Taylor [10] it is useful to start the discussion with a brief summary of these results. Their scaling relation is identical in form to those given by Eqs. (8), (9) and (10) corresponding to Suydam marginal stability and classical transport. The Connor-Taylor scaling for τ_E is derived on the basis of dimensional invariance of the scaling relations under any transformation that leaves the equations regulating plasma evolution themselves invariant. They applied their method to the RFP as well as other configurations. To complete their scaling for τ_E additional information was required concerning the nature of the turbulence. Specifically, for the RFP, transport was assumed to be determined by resistive g-mode activity, leading to the scaling law for τ_E given by Eq. (8). Furthermore, the same approach predicts a scaling for β_p (in an ohmically heated RFP) that is independent of I, N, and a as long as radiation is not important. This is in agreement with Eq. (9).

The derivation of Connor-Taylor scaling relies on the early resistive MHD dispersion relation (see Ref. [11]), which uses the adiabatic energy equation and neglects heat conductivity. Thus, "g-modes" are always present, which are then assumed to dominate plasma turbulence. In terms of plasma turbulence, the Connor-Taylor scaling corresponds to the following dependence of magnetic fluctuations with the Lunquist number

$$B_{1r} \sim S^{-0.5} \tag{19}$$

which can be compared with the experimental relation given by Eq. (15). The $S^{-0.5}$ dependence leads to a much more optimistic scaling law for confinement in an RFP, because of its strong dependence on the current I. Recent

targeted experimental campaigns, performed mostly on MST (see Ref. [2]), and less on RFX, have demonstrated a much less favorable dependence of τ_E versus I (as seen in the previous section) then the Connor-Taylor scaling.

B Werley's observation

Although the Connor-Taylor relation is not very reliable for predicting the dependence of τ_E with I, N, and a on a given device, Werley observed a remarkable agreement relating the best performance of different devices [1]. Specifically, Werley observed that using a restricted database made up of only the "best" confinement discharges provided by each individual RFP device the corresponding values of τ_E closely fit the Connor-Taylor scaling.

This result could be potentially very important to the RFP community, since it predicts that when operating at peak performance, RFP devices drastically improve their confinement as the size and hence plasma current increases. Given the importance of this result by Werley et al, it is worthwhile to see whether it can be recovered in the context of the present analysis and the very recent results on RFP confinement.

The key issue is the definition of "best" performance. In Table 6, confinement data from the RFP International Database are listed, exactly as reported in Ref. [1]. A multiple linear regression allows one to confirm that this special database indeed follows Connor-Taylor scaling (see Fig. 10)

$$\tau_E \simeq 5.8 \cdot 10^{-3} \cdot \frac{I^{3.05} \cdot a^{1.72}}{N^{1.62}} \quad [sec] \tag{20}$$

where the units are $I[MA]$, $a[m]$, $N[10^{20} m^{-1}]$.

C Reconciling the differences

The point that is addressed here is to investigate how this result fits with the apparently very different scaling law found in the present paper. As stated, the key issue concerns the proper characterization of the best confinement discharge for each individual device.

A plausible interpretation comes from an equivalent RFP "Greenwald limit". This limit suggests that there is a maximum density (whose value depends upon the plasma current) attainable by the plasma before its confinement is seriously degraded, for example due to enhanced radiation effects or even a disruption. Defining this maximum density as N_{best}, it is then

reasonable to postulate that the best confinement discharge corresponds to machine operation at the best density N_{best} for a given current. A multiple linear fit of the density in Table 6 with current and minor radius leads to the following general scaling (see Fig. 11)

$$N_{best} \simeq 0.713 \cdot I^{1.50} \cdot a^{-0.063} \tag{21}$$

(for comparison, the tokamak Greenwald limit in these units ($10^{20} m^{-1}$) is given by $N_{best} = I$). Note that the dependence of N_{best} with the minor radius a is indeed very weak; nonetheless, the dependence with the current is not linear, as the tokamak Greenwald limit would suggest, but a bit stronger. Substituting Eq. (21) into Eq. (20), leads to the following scaling relation for best confinement discharges

$$\tau_E \simeq 9.85 \cdot 10^{-3} \cdot I^{0.62} \cdot a^{1.82} \quad [sec] \tag{22}$$

It is now possible to directly compare this scaling relation with the one obtained in the present paper (see Fig. 12); in particular, substituting Eq. (21) for the density into Eq. (6), yields the scaling relation for the best confinement discharges, as predicted by the resistive MHD transport model

$$\tau_E \simeq 10^{-2} \cdot I^{0.72} \cdot a^{1.62} \quad [sec] \tag{23}$$

showing reasonably good agreement with Eq. (22). Note that the numerical coefficient in Eq. (23) is given by the model as a function of the pinch parameter Θ. Since the experimental values for Θ are not reported in the RFP International Database for best confinement shots, the coefficient in Eq. (23) is calculated for $\Theta \sim 1.7$; the weak dependence of τ_E upon the pinch parameter ensures good accuracy in the estimation of the numerical coefficient.

A few final comments are in order concerning the data in Table 6. First, keep in mind that only seven data points have been used to extract the scaling relations in Eqs. (20) and (21). Moreover, the accuracy of these data, expecially for the early experiments, is characterized by large error bars. This prevents a similar analysis of β_p to be carried out, because of the high uncertainty in the measured values of plasma beta in the early experiments. Values from the newer devices, namely MST and RFX, are the most reliable in the database. It should also be noted that even though the shots used in Table 6 for MST and RFX describe good confinement in standard RFP

plasmas, it has yet to be verified that they indeed truly represent the best confinement found in these machines. Even so, the dependence of τ_E on I observed so far in both RFPs is quite weak and hence does not affect the conclusions very much. A final comment concerns two "best discharges" that were originally included in the RFP International Database, both belonging to an early Japanese device, TPE-1RM. These discharges were omitted from this analysis, because they are the only ones that clearly violate the (empirical) rule that optimum scaling is obtained near the Greenwald density limit (see Ref. [1]); that is, their best performance does not occur at the RFP Greenwald limit.

VII Comparing an RFP with a Tokamak

The last topic of interest concerns the implications of the present scaling laws to larger RFP's and how they would compare with a tokamak. Admittedly such comparisons are not unique and depend upon a number of assumptions. Even so the results can serve as a general guideline when attempting to foresee the future. In the discussion below a comparison is made of the predicted values of $nT\tau$ for a tokamak and an RFP as determined by the appropriate scaling laws. Once these formulae are derived it becomes straightforward to compare the predicted fusion performance of future devices.

A $nT\tau$ for a tokamak

The scaling of $nT\tau$ in a tokamak is obtained by using the ITER-89P L-mode scaling relation for τ_E and the power balance relation. The ITER-89P expression for τ_E is well known [12] and can be written as

$$\tau_E = 0.048 \frac{I^{0.85} R^{1.2} a^{0.3} k^{0.5} n^{0.1} B^{0.2}}{P^{0.5}} \quad [sec] \tag{24}$$

where k is the elongation, P is the total heating power in $[MW]$, B is the toroidal field and the units are $I[MA]$, $a[m]$, $n[10^{20} m^{-3}]$, $B[T]$. An expression for the power is obtained from the power balance relation

$$\frac{3}{2} \frac{nT}{\tau_E} = \frac{P}{2\pi^2 R a^2 k} \tag{25}$$

or in practical units

$$P = 0.47\frac{kRa^2nT}{\tau_E} \tag{26}$$

Combining Eqs. (24) and (26) yields the desired relation

$$nT\tau = 2.0 \cdot 10^{-3}\frac{q_*^{0.4}}{k^{0.4}}\left(\frac{R}{a}\right)^{1.8}\left[\frac{I^{2.1}N^{0.2}}{a^{0.8}}\right] \quad [10^{20}m^{-3}\ keV\ sec] \tag{27}$$

where $q_* \equiv 5a^2kB/IR$. If the best performance occurs at the Greenwald limit, which in present notation is given by $N[10^{20}m^{-1}] = kI[MA]$, then the peak value of $nT\tau$ is given by

$$nT\tau = 1.7 \cdot 10^{-2}\frac{I^{2.3}}{a^{0.8}} \quad [10^{20}m^{-3}\ keV\ sec] \tag{28}$$

for $q_* = 2$, $k = 1.6$, and $R/a = 3$. This is the desired expression.

B $nT\tau$ for an RFP

A similar analysis can be carried out for the RFP using the basic scaling relations for τ_E and β_p derived from the resistive MHD marginal stability model. These expressions can be written as (in standard units)

$$\tau_E \simeq 9 \cdot 10^{-3}\frac{I^{1.1}a^{1.6}}{N^{0.25}} \quad [sec] \tag{29}$$

$$\beta_p \simeq 7 \cdot 10^{-2}\frac{N^{0.49}}{I^{0.75}a^{0.16}} \tag{30}$$

From these expressions it is straightforward to construct the expression for $nT\tau$:

$$nT\tau = 6.2 \cdot 10^{-4}\frac{N^{0.24}I^{2.35}}{a^{0.56}} \quad [10^{20}m^{-3}\ keV\ sec] \tag{31}$$

If one now assumes that the best performance occurs at the Greenwald limit, which reduces to $N[10^{20}m^{-1}] = I[MA]$ (and is close to the empirical scaling from the limited RFP data available), then the peak value for $nT\tau$ for an RFP reduces to

$$nT\tau = 6.2 \cdot 10^{-4}\frac{I^{2.59}}{a^{0.56}} \quad [10^{20}m^{-3}\ keV\ sec] \tag{32}$$

This is the desired expression for an RFP.

C Comparison of an RFP with a tokamak

A comparison of Eq. (32) for the RFP and Eq. (28) for the tokamak shows, perhaps surprisingly, that the best performance as measured by $nT\tau$ scales nearly identical with I and a. The main difference is in the numerical coefficient in front which is about 30 times larger for the tokamak. The conclusion, which has been well known experimentally for many years, is that tokamak confinement is much more favorable than that in an ohmically heated RFP. The RFP community is well aware of this observation and in recent years considerable efforts, which have been met with a high level of success, have been devoted to improving RFP confinement by non-ohmic means. The effort to further improve confinement remains as a major challenge in RFP research.

VIII Summary

The resistive MHD marginal model described here explicitly predicts the anomalous transport coefficient for perpendicular thermal diffusivity in a self-consistent manner by imposing the marginal stability condition on an ohmically driven Taylor-like relaxed state. In a sense, the present calculation proceeds inversely from traditional transport models, where the profiles are evaluated from the transport coefficients. Here $\chi_\perp$ is evaluated from the marginally stable temperature profile. Classical values for parallel thermal diffusivity and plasma resistivity have been chosen in the model. Anomalous parallel transport may be important in an RFP, but from a physical point of view even the classical value of $\chi_{||}$ is enormously large compared to the perpendicular value. Moreover, in the marginal stability condition, only the ratio of parallel to perpendicular diffusivity to the one quarter power enters, so the sensitivity of the model to these parameters is relatively low.

Typical values of $20 - 60 m^2/s$ for the anomalous $\chi_\perp$ in the core region are found from simulating standard RFP discharges. These values exceed the classical value of $\chi_\perp$ by about two orders of magnitude. It would be interesting to have a more targeted experimental campaign trying to verify this result, as well.

The macroscopic scaling relations found with the 1D transport model presented here agree reasonably well with recent experimental and computational results, showing a less optimistic scaling law for confinement in an

ohmic RFP than Werley's best performance observation. In particular, a weaker dependence of τ_E upon the plasma current is found, which is an important issue for the future large RFP fusion experiments. In comparison with previous work, the results found with the present model provide considerably more detailed information on the scaling relations. These relations are obtained by independently varying both the plasma current I and the area-integrated density N, which was not possible in the previous scaling relations. It is worth noting that only the MST device has confinement data obtained with independent values of I and N. Such data is not currently available from other devices. The marginal stability model allows a comparison of multiple discharges from a single machine, showing reasonably good agreement in terms of global parameters for MST. The present model also gives the scaling of plasma confinement with two other important parameters: the minor radius and the pinch parameter Θ. A weak dependence on Θ is found, in agreement with experimental observations. However, a quite significant dependence of τ_E versus the minor radius has been found (see Eq. (6)).

In conclusion, the scaling laws found with the resistive MHD marginal stability transport model agree reasonably well with experimental data and computational modeling. When extrapolated to the future, the present scaling relations imply that proposed reactor concepts (NEPI and TITAN) would have difficulty reaching their design goals (breakeven and ignition) if operated as a purely ohmic RFP. The suggestion is to maintain the effort concerned with exploring improved confinement by new techniques aimed at reducing the turbulence in an RFP. A few techniques are already being used in modern devices (edge profile control, PPCD). Others are still being developed (Oscillating Current Drive). Indeed some significant improvement in confinement has already been observed (in MST, profile control increases τ_E by almost one order of magnitude). The present theory implies that one or more of these techniques should be successfully developed if the RFP is to become competitive with the tokamak as a fusion reactor.

References

[1] K. A. Werley, J. N. DiMarco, et al. *Nucl. Fusion*, **36**:629, 1996.

[2] M. R. Stoneking, S. T. Chapman, et al. *Phys. of Plasmas*, **5**:1004, 1998.

[3] D. Terranova et al. *Plasma Phys. Control. Fusion*, **42**:843, 2000.

[4] S. I. Braginskii. In *Reviews of Plasma Physics*, volume **1**. Consultants Bureau, NY, 1965.

[5] D. Bohm. *The Characteristics of electrical discharges in magnetic fields.* McGraw-Hill, NY, 1949.

[6] J. Scheffel and D. D. Schnack. *Nucl. Fus.*, **40**:1885, 2000.

[7] A. B. Rechester and M. N. Rosenbluth. *Phys. Rev. Lett.*, **40**:38, 1978.

[8] N. Mattor. *Phys. Plasmas*, **3**:1578, 1996.

[9] B. E. Chapman et al. *Phys. Rev. Lett.*, **87**:205001, 2001.

[10] J. W. Connor and J. B. Taylor. *Phys. Fluids*, **27**:2676, 1984.

[11] B. Coppi, J. M. Greene, and J. L. Johnson. *Nucl. Fusion*, **6**:101, 1966.

[12] P. N. Yushmanov et al. *Nucl. Fus.*, **10**:1999, 1990.

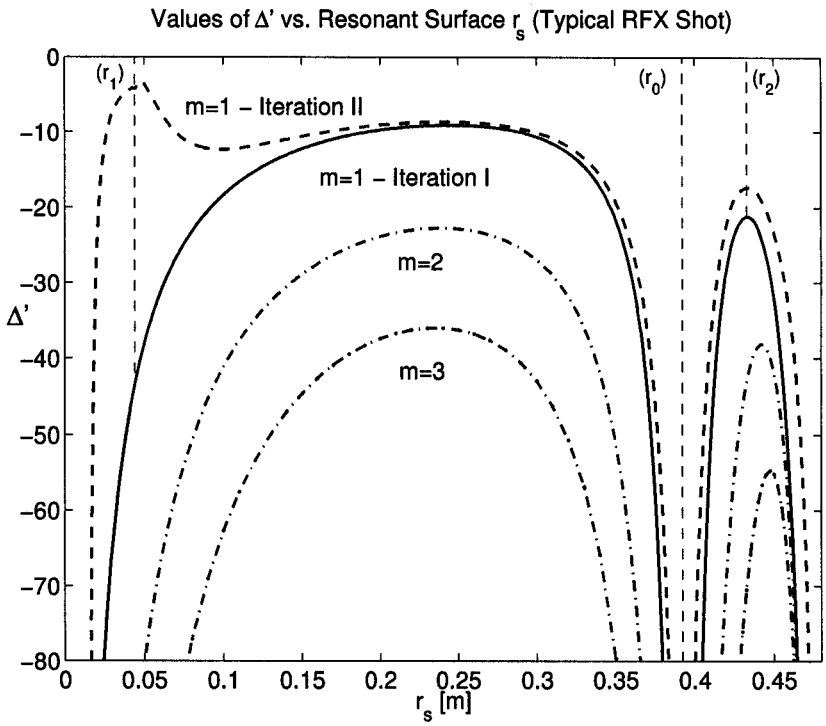

Figure 1: Illustration of the Transport Model Iterative Solving Procedure

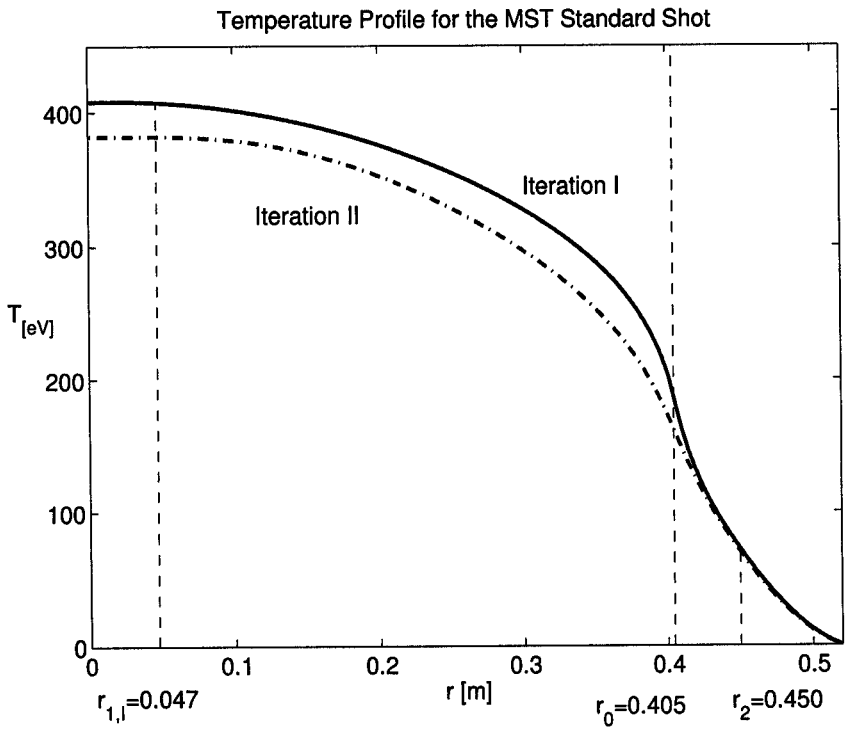

Figure 2: Tearing-Mode Marginally Stable Temperature Profile for MST Standard Shot

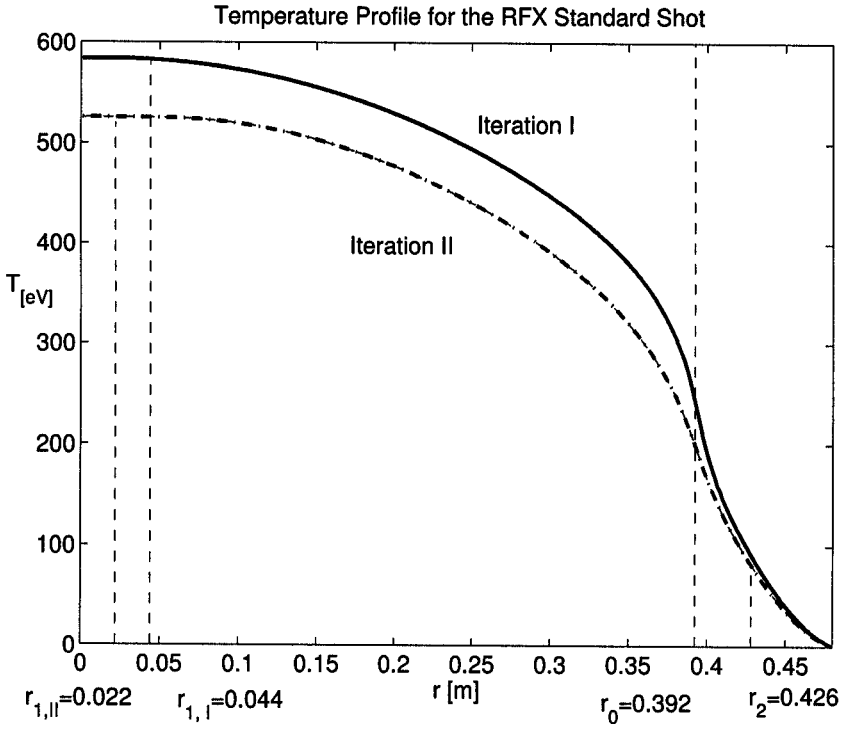

Figure 3: Tearing-Mode Marginally Stable Temperature Profile for RFX Standard Shot

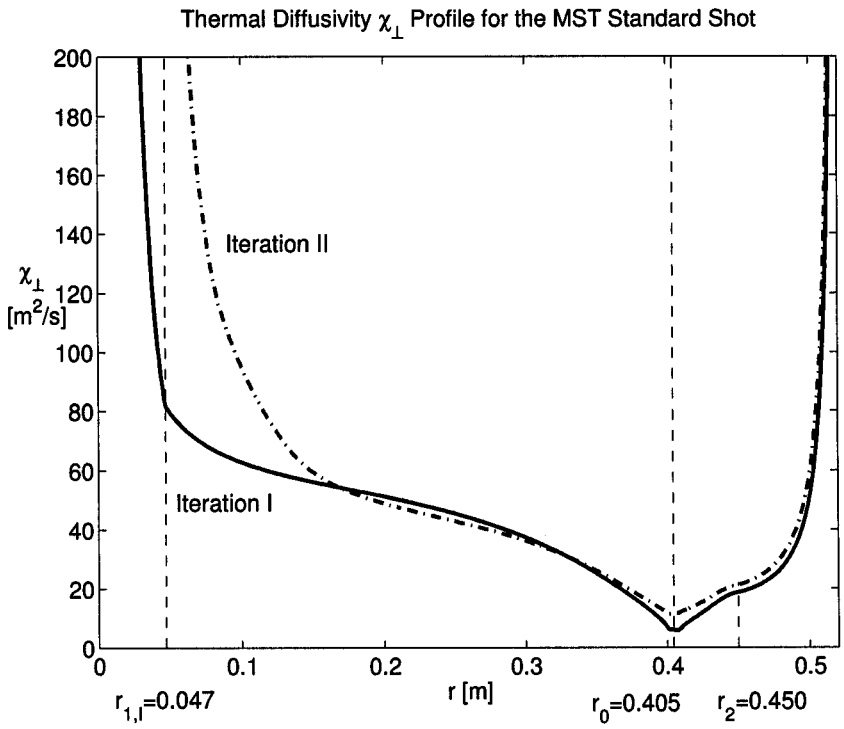

Figure 4: Tearing-Mode Marginally Stable $\chi_\perp$ Profile for MST Standard Shot

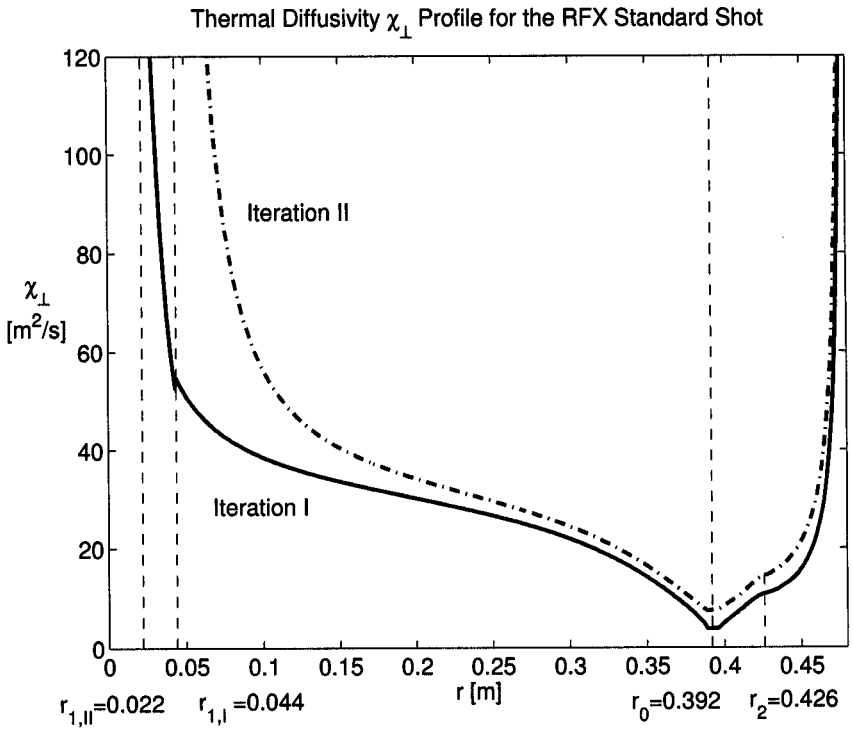

Figure 5: Tearing-Mode Marginally Stable $\chi_\perp$ Profile for RFX Standard Shot

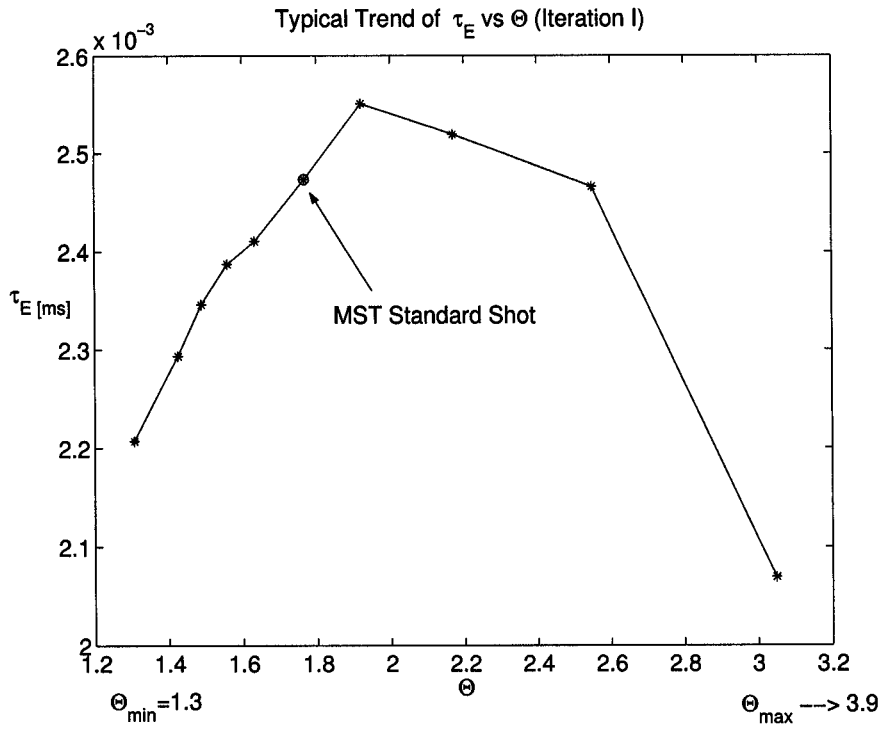

Figure 6: Θ Dependence of τ_E in the Tearing-Mode Marginality Scaling Law from Iteration I

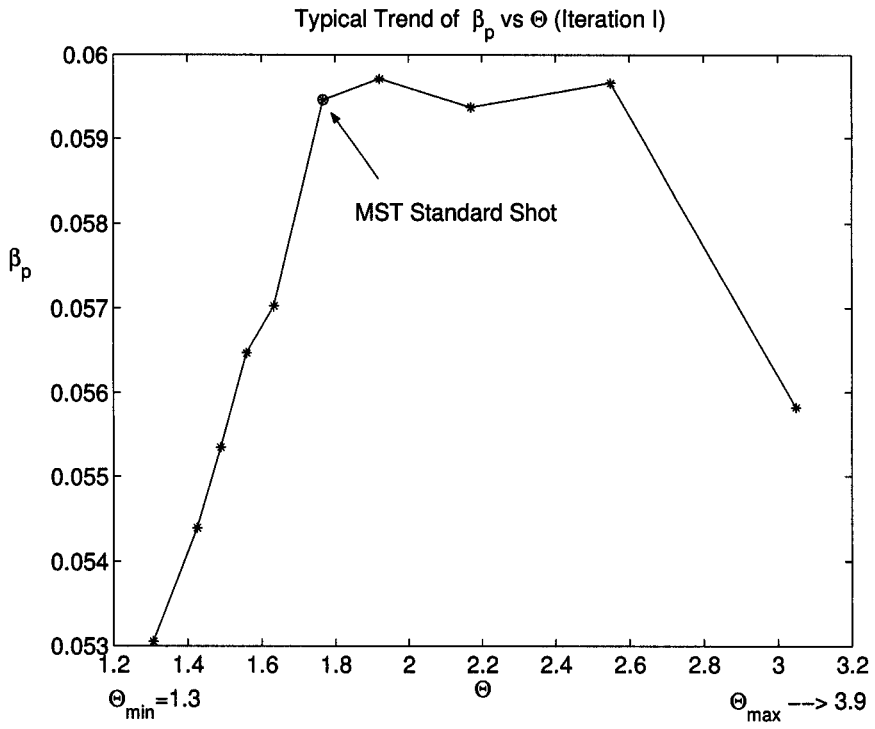

Figure 7: Θ Dependence for β_p in the Tearing-Mode Marginality Scaling Law from Iteration I

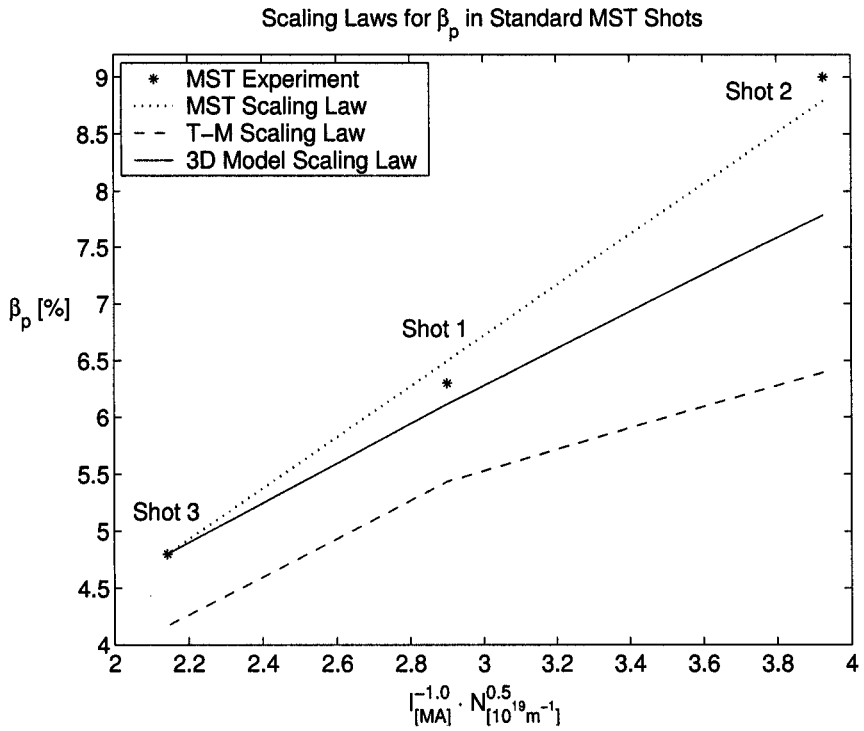

Figure 8: Comparison of Scaling Laws for β_p for MST Standard Shots

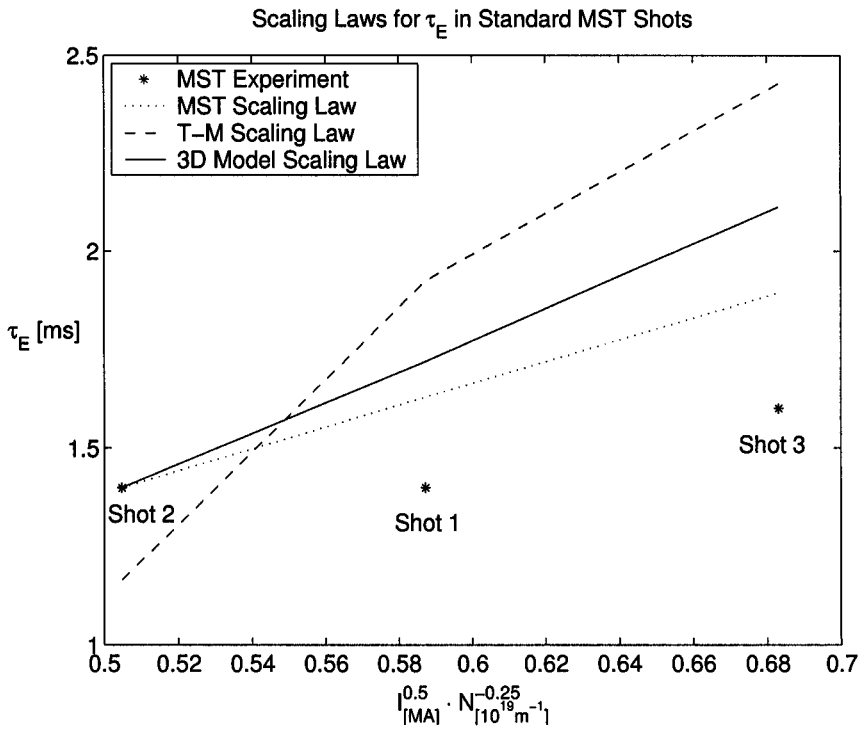

Figure 9: Comparison of Scaling Laws for τ_E for MST Standard Shots

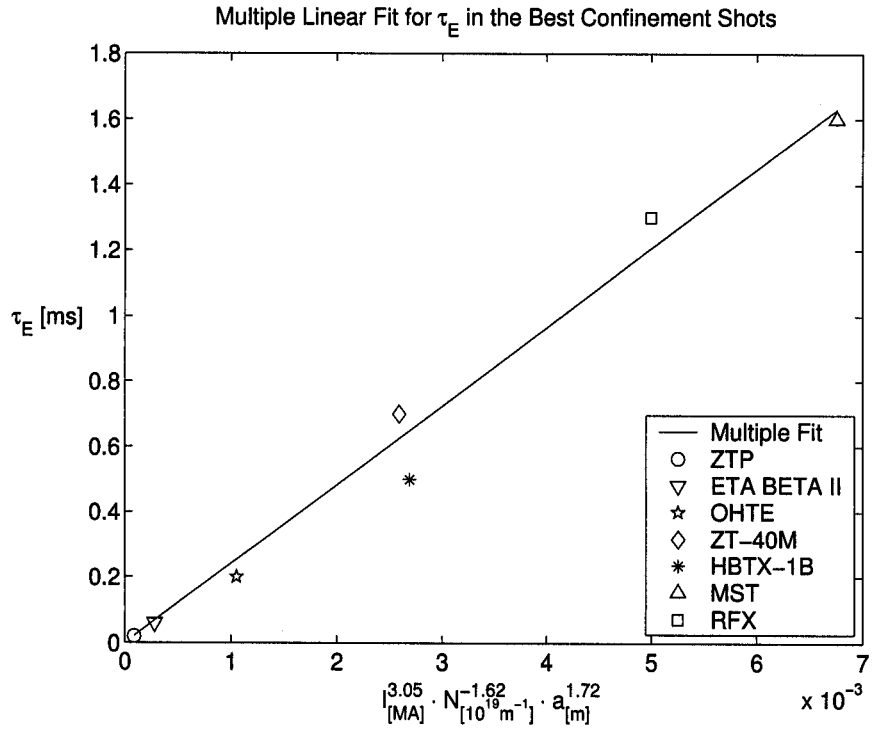

Figure 10: Scaling Law for τ_E extracted from RFP International Database of Best Confinement Shots

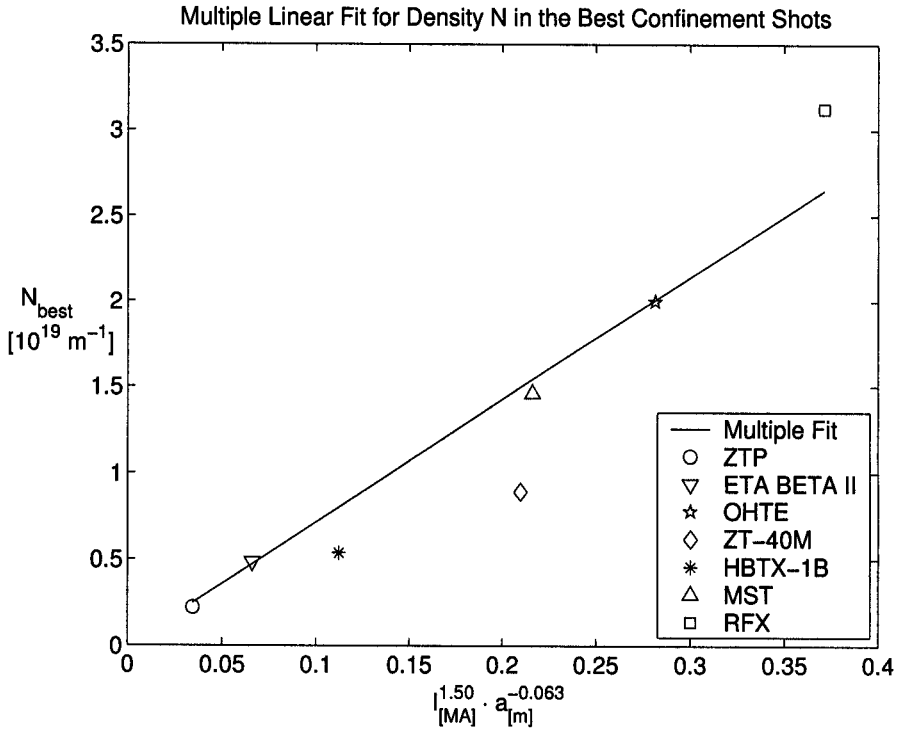

Figure 11: Scaling Law for N_{best} extracted from RFP International Database of Best Confinement Shots

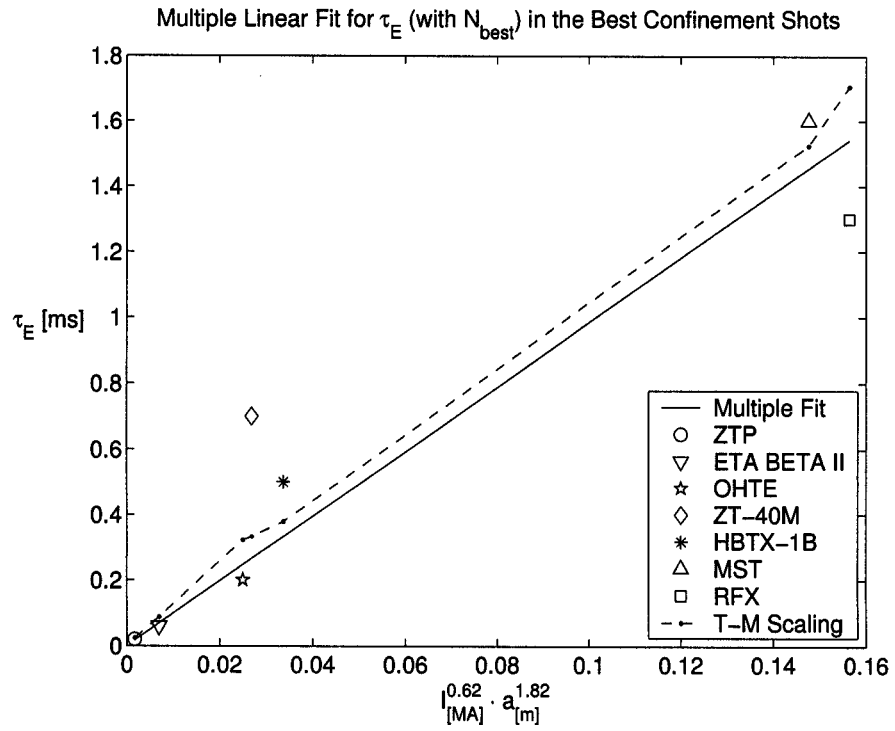

Figure 12: Scaling Law for τ_E at the highest possible density N_{best}, from the RFP International Database, compared with the tearing-mode transport model

Device	a $[m]$	I $[MA]$	Φ_t $[Wb]$	n_0 $[10^{20}m^{-3}]$	F	Θ	r_0 $[m]$	β_p [%]	τ_E $[ms]$
MST	0.52	0.376	0.0696	0.14	-0.22	1.77	0.418	6.29	1.38
RFX	0.48	0.5/1	0.12/0.16	0.2/0.5	0/-0.4	1.5/1.7	0.38	5	0.5/1.5

Table 1: Plasma Parameters in Typical RFPs Standard Shots for MST and RFX

Device	$I[MA]$	$\Phi_t[Wb]$	$n_0[10^{20}m^{-3}]$
MST	0.376	0.0696	0.14
RFX	0.750	0.141	0.35

Table 2: Plasma Parameters Held Fixed in the Simulation of RFPs Standard Shots

///	MST	Tearing-Mode	Suydam	Classical
///	Standard Shot	Marginality	Marginality	Transport
$\beta_p[\%]$	6.3	5.3	19.3	21.3
$\tau_E[sec]$	$1.4 \cdot 10^{-3}$	$2.0 \cdot 10^{-3}$	$41.0 \cdot 10^{-3}$	$37.4 \cdot 10^{-3}$

Table 3: Plasma Confinement Parameters For the MST Standard Shot

/// ///	RFX Standard Shot	Tearing-Mode Marginality	Suydam Marginality	Classical Transport
$\beta_p[\%]$	5	4.0	17.4	19.8
$\tau_E[sec]$	$0.5/1.5 \cdot 10^{-3}$	$2.4 \cdot 10^{-3}$	$43.4 \cdot 10^{-3}$	$57.1 \cdot 10^{-3}$

Table 4: Plasma Confinement Parameters For the RFX Standard Shot

///	$I[MA]$	$N[10^{19}m^{-1}]$	$\beta_p[\%]$	$\tau_E[ms]$
Shot 1	0.376	1.2	6.3	1.4
Shot 2	0.210	0.68	9.0	1.4
Shot 3	0.430	0.85	4.8	1.6

Table 5: Plasma Parameters for the MST Standard Shots used in Fig. 8 and Fig. 9

///	$I[MA]$	$N[10^{19}m^{-1}]$	$a[m]$	$\tau_E[ms]$
ZTP	0.095	0.221	0.068	0.02
ETA BETA II	0.150	0.484	0.125	0.06
OHTE	0.400	2.00	0.18	0.20
ZT-40M	0.330	0.892	0.20	0.70
HBTX-1B	0.220	0.537	0.26	0.50
MST	0.350	1.458	0.50	1.60
RFX	0.500	3.125	0.457	1.30

Table 6: RFP International Database, as reported in Ref. [1]